Journal of
Ceramic Science
and Technology

J. Ceram. Sci. Technol., **09** [2] 119-126 (2018)
DOI: 10.4416/JCST2017-00085
available online at: http://www.ceramic-science.com

High-Temperature Measurements of Macroscopic Deformation Induced by Phase Changes: Application to Bauxite-Based Material

A. Coulon[1], E. de Bilbao[*1], S. Brassamin[1], J. Poirier[1]

[1]CNRS, CEMHTI UPR3079, Univ. Orléans, F-45071 Orléans, France

received November 6, 2017; received in revised form January 3, 2018; accepted January 22, 2018

Abstract

High-temperature measurements of macroscopic deformation are of great interest for better understanding the behaviour of materials used in high-temperature processes. However, such measurements are still challenging when performed on very heterogeneous materials such as the bauxite-based material studied here. In this work, a high-resolution camera is used in combination with a high-temperature furnace to monitor the change in size of a bauxite-based sample. The technique is applied to measure the change in diameter induced by phase transformation of the material and by the impregnation of molten oxides. The decrease in diameter owing to solid-liquid sintering has been assessed to 5 % and the formation of the expansive phases $CaO{\cdot}6(Al_2O_3,Fe_2O_3)$ and $CaO{\cdot}2(Al_2O_3,Fe_2O_3)$ makes the diameter increase by 0.5 and 5 %, respectively. It is also possible to identify the temperatures at which the transformations occur. The technique may be used to study the effect of corrosion on macroscopic deformation of refractories.

Keywords: Refractory materials, contactless measurement, deformation, high temperature, phase transformation

I. Introduction

Volume expansion induced by phase changes has been studied for a long time in the field of ceramics and composites[1–8]. Routinely used, thanks to their high accuracy, classic dilatometers allow the determination of the coefficient of thermal expansion, shrinkage induced by sintering, glass transition, and chemical changes[4,9–10]. Contactless optical instruments have pushed the temperature limit back and can therefore be used in the measurement of melting samples[11–13]. However, the sample size limitation to a few millimetres makes it difficult to conduct tests on heterogeneous material with a large representative volume. For instance, some refractory materials are made of aggregates measuring a few millimetres and a representative volume must have a characteristic dimension larger than a few centimetres. Furthermore, high-temperature transformation of raw materials is another case where the aggregates may have a size of a few millimetres. The usual apparatus is not appropriate for these materials.

De Bilbao *et al.* performed accurate 3D measurements of the macroscopic deformation of SiC-based refractory castables induced by slag corrosion and to relate the deformation to the phase changes [14, 15]. The measurements were performed at room temperature before and after the corrosion test. Merzouki *et al.* also performed accurate measurements of the swelling of SiC-based refractory castables induced by oxidation [16]. The authors used a calliper to measure the diameter of the sample every millimetre over the height at high temperature at the beginning and at the end of the dwell. However, neither method combined high spatial resolution with real-time *in-situ* measurement.

The current work was aimed at determining, at high temperature, the macroscopic change in the volume of a heterogeneous sample composed of aggregates measuring a few millimetres in size induced by the sample's own phase changes or in contact with molten oxides and relating the deformation to the phase transformations. To achieve these objectives, *in-situ* optical measurement of deformation method was thought to be relevant. The technique is based on the determination of the change in diameter of a cylindrical sample over its height from post-processing images. However, commercial optical devices, such as optical dilatometers or hot stage microscopes, do not allow for testing sample sizes exceeding few millimetres. Additionally, sample size and resolution decrease when the test temperature increases. This motivated us to develop a specific device. A standard furnace has been equipped with a wide quartz window that makes it possible to capture images with a high-resolution camera at high temperature. The main merits of this device are first the possibility to perform *in-situ* high-temperature measurements and second the possibility to test larger samples than is possible to test with commercial optical dilatometers. Macroscopic deformations are evaluated by means of image processing. X-ray diffraction and scanning electron microscopy analyses were performed on the samples after the tests to determine the phase changes. Our approach was applied to samples made of coarse aggregates of bauxite. Two tests were performed. The first one was carried out on the sample alone to measure the deformation induced by the phase changes of the sample itself. In the second test, pellets of

* Corresponding author: emmanuel.debilbao@univ-orleans.fr

oxides were placed on the top of the sample to study the effect of reactive impregnation. Additionally, image processing was performed on the area corresponding to the molten oxides that had not yet impregnated the sample to evaluate the impregnation rate.

II. Material and Methods

1. *Materials*

Bauxite is used as a raw mineral and as a raw refractory material in many industries. At high temperature, bauxite-based mineral undergoes phase changes such as dehydration of diaspore, decarbonation, and formation of calcium-aluminates phases [17], which may induce significant changes in volume. Bauxite-based raw materials are characterized by:

- High heterogeneity owing to aggregates measuring a few millimetres in size
- Phase changes at high temperature with formation of liquid phase
- Large macroscopic deformation

These characteristics make it difficult or even impossible to measure deformations at high temperature using classic dilatometers or contactless optical instruments. Bauxite-based materials are therefore a good example for the application of the *in-situ* measurement method presented in this paper.

Bauxite samples were composed of red bauxite aggregates (Ø ≤4 mm) mixed with a mineral molten phase (Table 1). The molten phase was composed of two lime-alumina phases, $CaO{\cdot}(Al_2O_3,Fe_2O_3)$ and $2CaO{\cdot}(Al_2O_3,Fe_2O_3)$, and gehlenite $2CaO{\cdot}Al_2O_3{\cdot}SiO_2$. Cylindrical samples measuring 30 mm in height and 28 mm in diameter were shaped by means of uniaxial compaction under a pressure of 16 MPa, and pre-fired at 500 °C. The open porosity was measured with the Archimedes' method using oil and ranged from 31 % to 35 %.

The molten oxides used for the second test were mixed to be close to the molten phase of the sample. They were mainly composed of Al_2O_3, CaO and Fe_2O_3 (Table 1). The mixture of oxides was compacted at room temperature to form pellets. The liquidus temperature, 1385 °C, and the solidus temperature, 1140 °C, were determined by means of differential scanning calorimetry (Setaram Ligne 96) with a heating rate of 5 K/min in an argon flow of 20 mL/min.

Table 1: Chemical composition of bauxite material and reactive molten oxide (±1 wt%)

	Al_2O_3	Fe_2O_3	CaO	SiO_2	TiO_2
Bauxite material	56	21	12	9	2
Molten oxides	40	14	38	6	2

2. *In-situ measurement device*

The device for optical measurement of deformation is composed of a high-temperature furnace (Thermoconcept HTL04, 1750 °C) with a window (40 × 50 mm²) integrated in the door (Fig. 1). The high-resolution CCD monochromatic camera (6579 × 4384 pixels), fitted with an SP70–300 mm lens (TAMRON), is positioned 80 cm from the furnace window. A UV-filter protects the camera against thermal radiation. Owing to the design of the door, the maximum sample size is 35 mm in width and 45 mm in height. This size is bigger than that of samples tested with commercial devices, such as optical dilatometers or hot stage microscopes (HSM), for which the sample size cannot exceed a few millimetres. Moreover, the maximum temperature 1750 °C is higher than that of available devices. The optical system was calibrated with a gauge block of 30 mm for each test. The pixel size was evaluated at 12 ± 1 µm, depending on the position of the sample and the optical adjustment. The uncertainty in diameter measurement depends on the initial sample geometry, i.e. size, cylindricity, waviness, roughness, and also on the temperature. Measurements of the coefficient of thermal expansion (CTE) of alumina-based samples showed that our technique overestimated the CTE up to 60 % compared with the results obtained with a classical horizontal dilatometer (Netzsch DIL 402 PC). For the application presented below, the diameter measurement uncertainty was ±0.05 mm for a diameter of 28 mm, i.e. ±0.35 %. This uncertainty was acceptable in respect of the observed deformations.

The cylindrical sample (h = 35 mm, Ø = 28 mm) was placed on two alumina rods and walls made of alumina slabs were placed around it to isolate the sample from the direct radiation of the furnace resistances (Fig. 2). The sample temperature was evaluated by means of a thermocouple placed right behind the sample.

Fig. 1: Photo showing the *in-situ* measurement device.

For all experiments, the sample was heated up to 1450 °C for 4 h in air with a heating rate of 300 K/h. An image of the

sample was taken at room temperature before heating. The reference intensity was calculated over a region of interest delimited by a rectangle framing the sample. The reference intensity was used to adjust the exposure time of the camera to keep the grey level gradient constant independent of the heating radiation. Images were captured every minute for a temperature lower than 1300 °C, and every 30 seconds above. Time and temperature were also recorded for each image. Finally, a last image was also taken at room temperature after the firing.

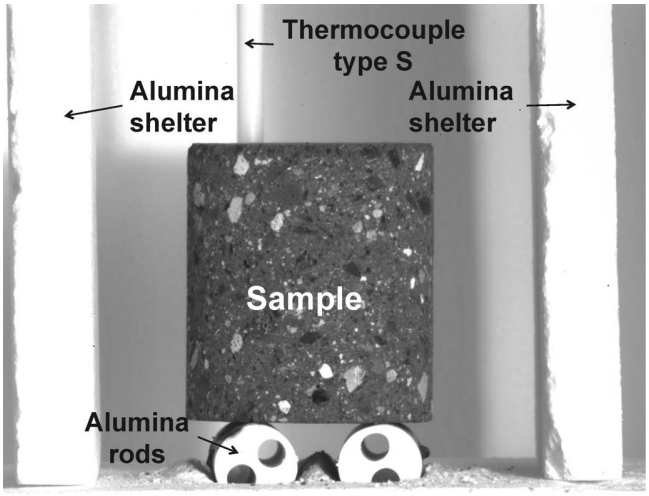

Fig. 2: Photo showing the sample placed on cylindrical alumina supports under an alumina shelter before firing.

After the experiment, the diameter of the sample was evaluated for each image by means of image processing. During the test, the rods supporting the sample expand owing to the heating. The vertical position of the sample is determined based on the edges of a vertical segment (red vertical line on Fig. 3). The edge detection is based on the grey level gradient. The vertical line is also used to measure the sample height and to distribute uniformly a chosen number of horizontal lines over the height of the sample. The diameter is evaluated for each horizontal line from the edge coordinates. It is then possible to calculate the mean diameter and to compare it with that of the initial image captured at room temperature. An equivalent profile can be also derived from the relative change in diameter line by line over the height.

3. Sample analyses

After the tests, the samples were cut along the main axis and prepared for scanning electron microscopy coupled with energy-dispersive X-ray spectroscopy (SEM-EDX, FEI ESEM XL40). The SEM-EDX analyses allowed mapping of phase contents over the height of the fired sample. The mapping was performed on a rectangular zone of interest, 1.5 mm in width, centred on the analysed surface to prevent edge effects. The zone was divided into a grid pattern made of rectangles, 0.8 mm high. Additionally, X-ray diffraction analyses (Bruker, D8 Advance) were performed on fired samples at room temperature to determine the crystalline phases. Thermodynamic calculations, performed with Factsage software [18] (FToxid database), completed the SEM-EDX and XRD results to determine the crystalline phases and liquid phase present at high temperature.

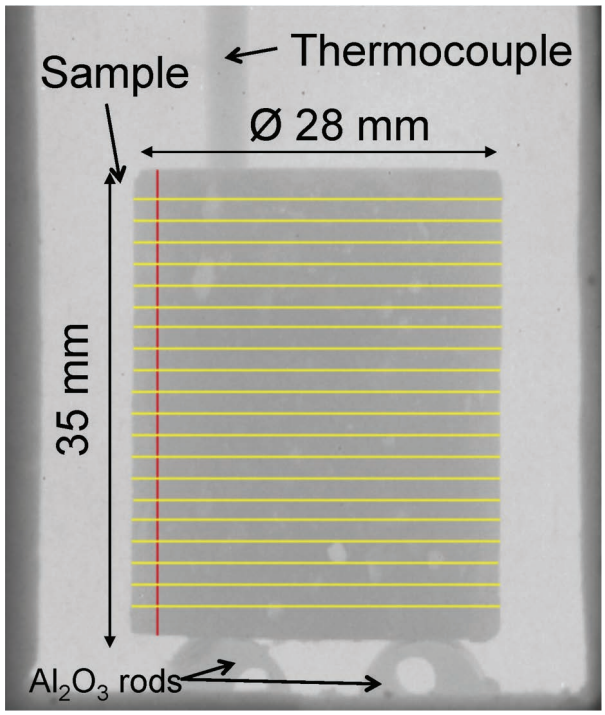

Fig. 3: Photo showing the sample taken at 1450 °C. Image processing consists of defining a vertical line using edge detection to assess the sample height. Horizontal lines are then uniformly distributed over the height. Each horizontal line gives an equivalent diameter and all the lines make it possible to draw an equivalent profile.

III. Results and Discussion

1. Measurement of the macroscopic deformation of the bauxite-based sample.

The first application of our method was aimed at measuring the deformation induced by the mineral phase changes of the bauxite-based sample itself. Apart from the first image, the camera started to capture images from 600 °C because of the lack of brightness below this temperature. Above 600 °C, sample radiation enhanced furnace radiation to get the brightness and contrast required for post-processing quality. Images captured while furnace resistance heating elements were on offered the best contrast. The diameter was determined on 20 horizontal lines and the mean relative change in diameter was derived from the initial mean diameter of the first image at room temperature. The measurement uncertainty of each edge coordinate was about 4 pixels, yielding an uncertainty of the diameter measurement of about 96 µm for a sample measuring 28 mm in diameter. This corresponded to a relative change in diameter uncertainty of ± 0.35 %.

The evolution of the relative change in the diameter of the sample during the firing is shown in Fig. 4. The green curve (triangles oriented upwards) corresponds to Line 3 located in the upper part of the sample while the blue one (triangles oriented downwards) corresponds to Line 15 located in the lower part. The red curve (diamonds) corresponds to the average relative change in the diameter of the sample (average of the 20 lines). The three curves can be split into five stages:

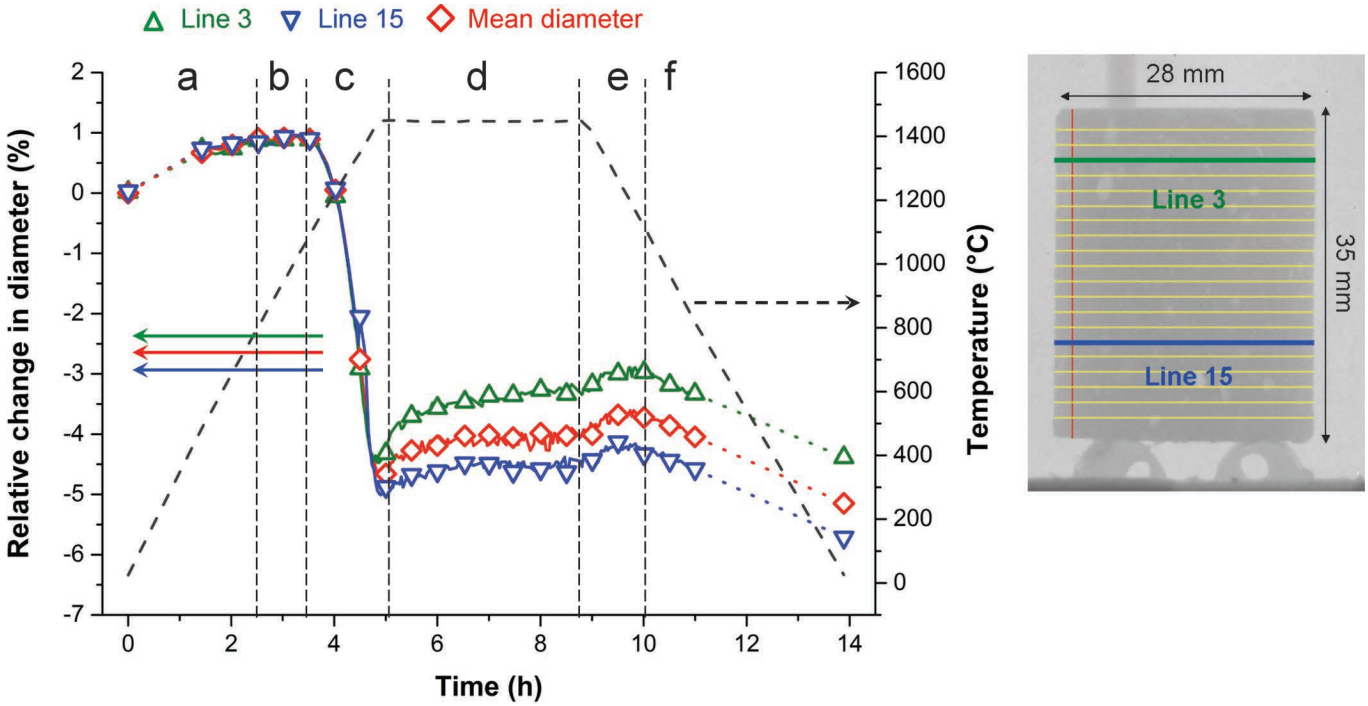

Fig. 4: Evolution of macroscopic deformation of the sample during firing. Section a corresponds to thermal expansion, Section b decarbonation of the material, Section c represents the shrinkage caused by reactive sintering, Section d corresponds to a reactive expansion, Section e represents the expansion caused by liquid solidification, and Section f corresponds to thermal expansion.

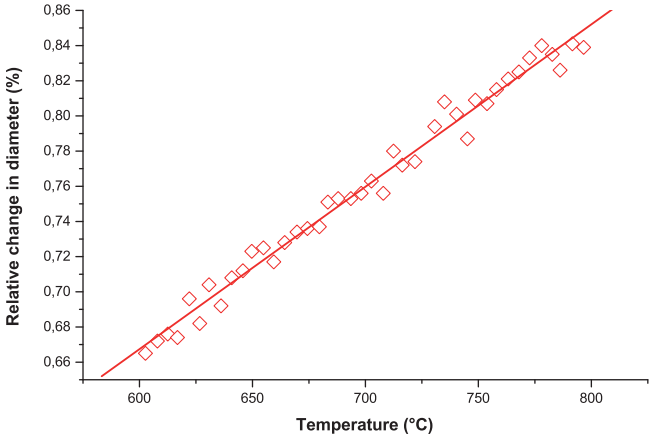

Fig. 5: Evolution of the change in diameter following the temperature from 600 °C to 800 °C. The thermal expansion coefficient was evaluated to 9.2 ± 1 × 10^{-6} K^{-1} with a coefficient of determination of 0.992.

Stages a and b: Previous investigation on this bauxite-based material showed that bauxite dehydrated at 500 °C but no phase change occurred from this temperature up to 800 °C [17]. Considering the first image was taken from 600 °C, the mean relative change in diameter is therefore due to linear thermal expansion, and the coefficient of thermal expansion between 600 and 800 °C was assessed to 9.2 × 10^{-6} K^{-1} (Fig. 5), which is in good agreement with the literature for bauxite [3]. From 800 °C the slope of the curve decreases slightly owing to decarbonation.

Stage c: From 1150 °C up to 1450 °C, the relative change in diameter decreases drastically with a drop of roughly 5 %. Secondary phases melted and reacted with the bauxite aggregates and the solid mineral binder, yielding a reactive sintering prevailing over the thermal expansion.

Stage d: When the temperature reached 1450 °C the shrinkage stopped and the sample started to swell especially within the first hour of the dwell. The swelling can be explained by the precipitation of the major phase $CaO{\cdot}6(Al_2O_3,Fe_2O_3)$ (80 wt%) observed in SEM-EDX and XRD analyses. No significant variation of the chemical composition was observed along the vertical axis, revealing the expansive phase precipitated uniformly within the sample in agreement with the rather uniform sample shape. Thermodynamics calculations confirmed that a liquid phase (20 wt%) formed at high temperature. The change in diameter owing to the precipitation of $CaO{\cdot}6(Al_2O_3,Fe_2O_3)$ was about 0.5 %.

Stage e: At the end of the dwell, the diameter increases during cooling down to 1250 °C owing to the solidification of the liquid phase.

Stage f: The sample continued to cool freely and the diameter decreases owing to thermal expansion.

It can be observed that the upper and lower lines (Fig. 4) show a difference in diameter change from the beginning of the swelling induced by the precipitation of hibonite. This could be explained by the heterogeneity of the sample composition.

2. Deformation of bauxite-based sample interacting with molten oxides

In this test, three pellets of pre-mixed oxides, representing 3.5 wt% of the sample weight, were put on the top of the sample before its insertion into the furnace. The test was performed in the same way as the previous one and the sample geometry was analysed as previously. Fig. 6 shows images of the sample with the pellets at four different temperatures: 1180, 1330, 1380, and 1445 °C.

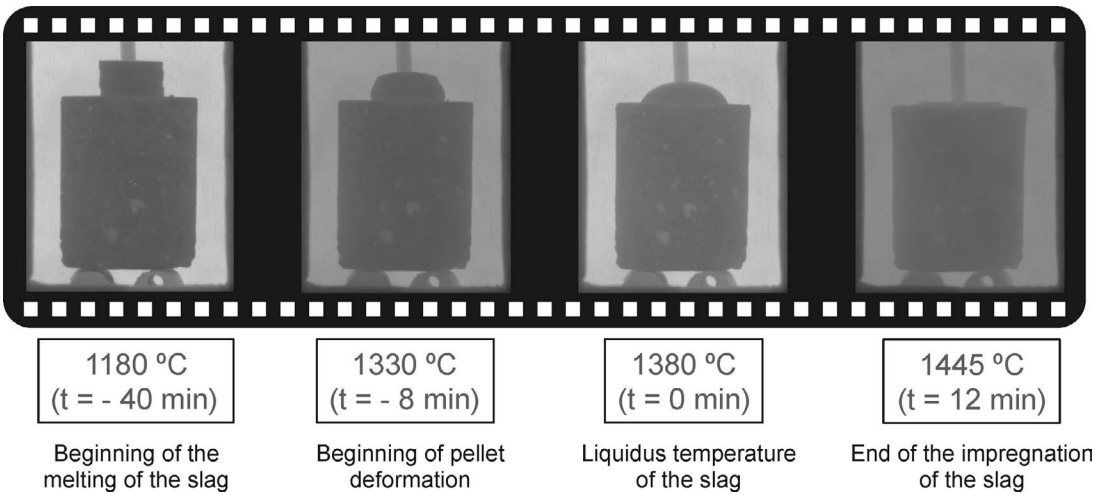

Fig. 6: Photos of the sample and pellets at different temperatures.

The pellets melted and wetted the sample from 1380 °C. They had disappeared at 1445 °C just before the plateau.

Micrographs of the sample facilitated understanding of the reactive impregnation occurring during the test (Fig. 7). The sample texture completely transformed in the upper zone. Aggregates dissolved, pore size increased significantly, and cracks formed. EDX analyses combined with thermodynamics calculations indicate the precipitation of $CaO{\cdot}2(Al_2O_3,Fe_2O_3)$ solid phase and a liquid phase at 1450 °C. The liquid phase composition was closed to CAS_2 with a low quantity of Fe_2O_3 (8 ± 1 wt%). In the lower zone, the texture and the microstructure of the sample were similar to those of the sample tested alone. $CaO{\cdot}6(Al_2O_3,Fe_2O_3)$ and liquid phase were observed as expected. The content of the liquid phase was higher than the content observed in the first test, even at the bottom. A part of the liquid phase produced by the oxide pellets wholly impregnated the sample. However, the interactions between the molten oxides and the sample in the upper zone differed from those in the lower zone. The mixture of oxides was mainly composed of Al_2O_3 and CaO with a ratio very close to the eutectic point of binary system and it is possible to draw an analogy with this binary system. The liquid reacted with the alumina aggregates according to a dissolution/precipitation process, forming monomineral layers of calcium aluminates around the alumina grains [19] (liquid/$CaO{\cdot}Al_2O_3$/$CaO{\cdot}2Al_2O_3$/$CaO{\cdot}6Al_2O_3$/Al_2O_3). For the system studied in this work, the reactivity of the slag with its initial composition was high and the liquid diffusion prevailed on the solid diffusion. The $CaO{\cdot}2(Al_2O_3,Fe_2O_3)$ layer grew instead of $CaO{\cdot}6(Al_2O_3,Fe_2O_3)$. The slag enriched in alumina remained liquid owing to the presence of silica, but its reactivity decreased. It barely reacted with the material. The formation of the $CaO{\cdot}6(Al_2O_3,Fe_2O_3)$ layer was mainly due to the liquid phase formed from the matrix of the sample itself as it was observed on the test without the pellets.

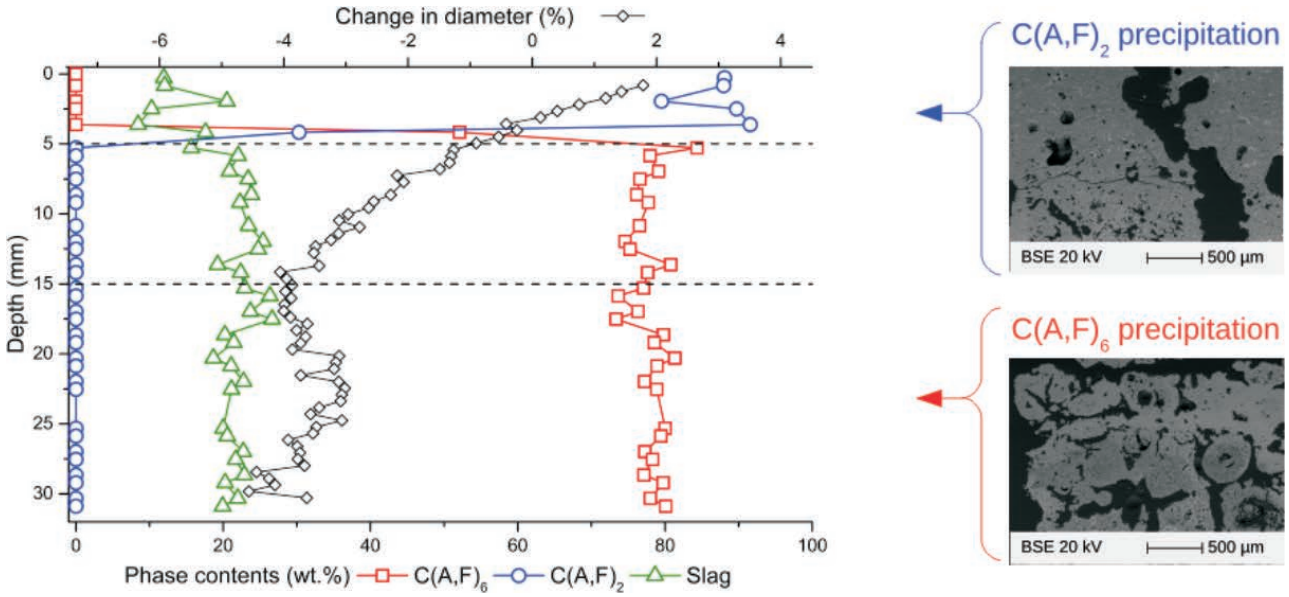

Fig. 7: Phase composition of the sample along the vertical axis after firing according to Factsage thermodynamic calculation from the MEB/EDX mapping. In the upper zone, the slag impregnated the sample and reacted to form $CaO{\cdot}2(Al_2O_3,Fe_2O_3)$-aggregates dissolved and pore size increased. In the lower zone, the microstructure looks like the one observed in the sample tested without the slag pellets. Enriched therefore in alumina and remaining liquid, the slag continued to impregnate the sample but its reactivity decreased. It barely reacted with the aggregates. The precipitation of $CaO{\cdot}6(Al_2O_3,Fe_2O_3)$ was mainly due to the liquid phase formed from the bauxite-based material itself.

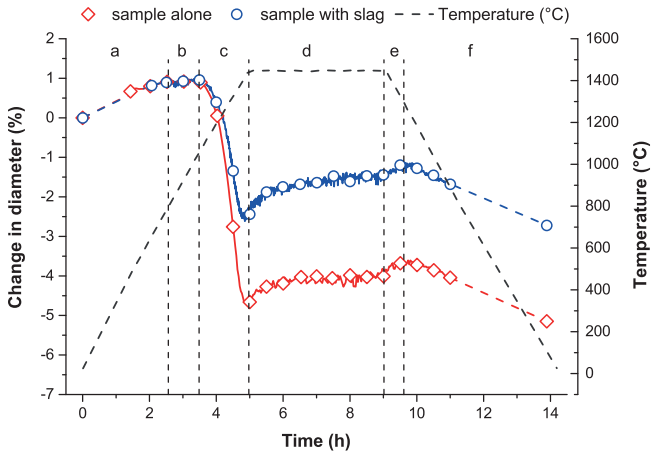

Fig. 8: Relative change in diameter. Comparison of change for sample without and with pellets.

The evolution of the average relative change in diameter of the sample interacting with the molten oxides was compared with that of a sample alone (Fig. 8). It can be observed that the evolutions are similar. However, the inflexion between the shrinkage stage and the swelling occurred earlier in presence of the pellets. The composition of the oxide pellets was close to the that of the liquid phase formed from the sample itself. The reactions with the aggregates were similar. However, the diameter decrease during the shrinkage stage was lower in the presence of the pellets. It can therefore be assumed that the change in diameter arising in the shrinkage stage results from both reactive sintering and swelling induced by the reaction. In the zone impregnated with the molten pellets, the reaction with aggregates started prevailing over the solid-liquid sintering earlier, mainly owing to the precipitation of the expansive phase $CaO{\cdot}2(Al_2O_3,Fe_2O_3)$. Moreover, the drop of the relative change in diameter increased during Stage d in comparison with the previous test since the phase $CaO{\cdot}2(Al_2O_3,Fe_2O_3)$ is more expansive than $CaO{\cdot}6(Al_2O_3,Fe_2O_3)$. According to calculation from the volumetric lattice parameter of the involved oxides $CaO{\cdot}6(Al_2O_3,Fe_2O_3)$, precipitation leads to a macroscopic expansion in volume of 3 % when precipitation of $CaO{\cdot}2(Al_2O_3,Fe_2O_3)$ expands the volume by about 24 %.

Moreover, the change in diameter along the vertical axis of the sample was not uniform (Fig. 9). The equivalent profile indicates the lower zone shrunk, like the entire sample in the test without the pellets. The slight difference at the bottom can be explained by the difference between the initial samples and the measurement uncertainties. On the contrary, the upper zone swelled. The expansion induced by the adding of molten oxides was more than two times higher than the chemical expansion observed on the sample tested alone. The lower zone shows a gradient of change in diameter along the axis although the phase composition does not change. This gradient can be explained by elastic deformation induced by the difference between the upper zone made of the more expansive phase and the bottom of the sample containing the less expansive phase.

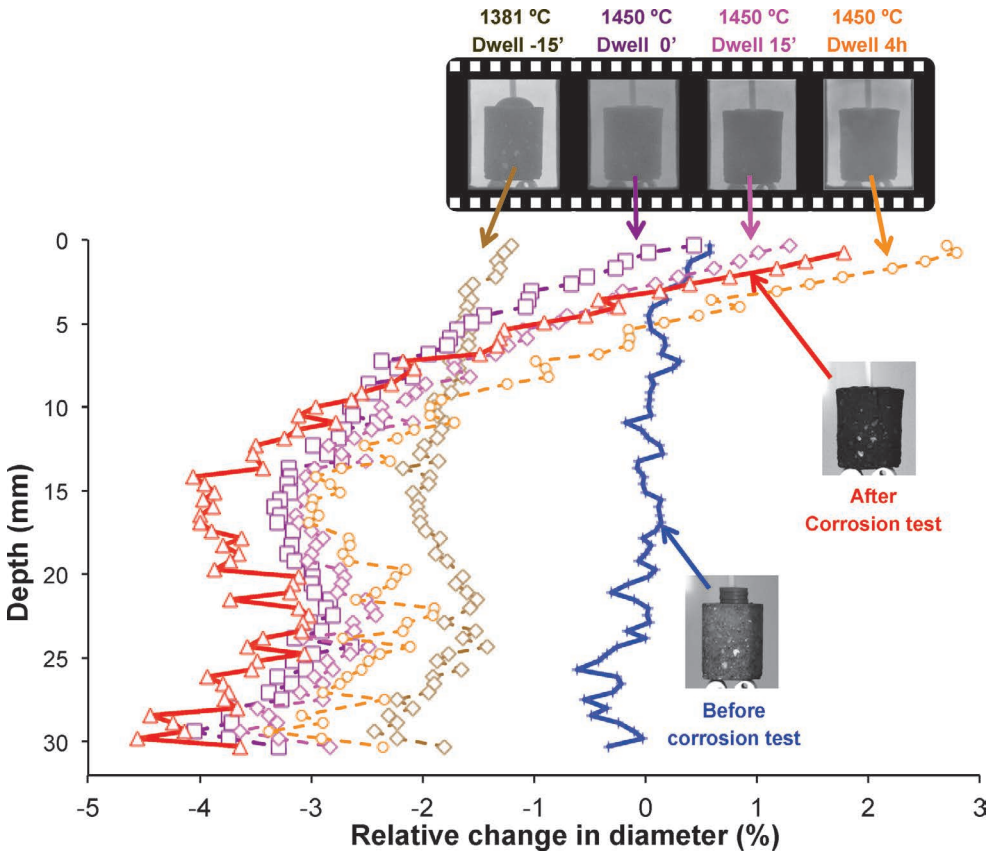

Fig. 9: Evolution of the relative change in diameter over the depth of the bauxite sample from the beginning of the impregnation and comparison of the relative change in diameter over the depth of before and after the corrosion test (blue line and red line).

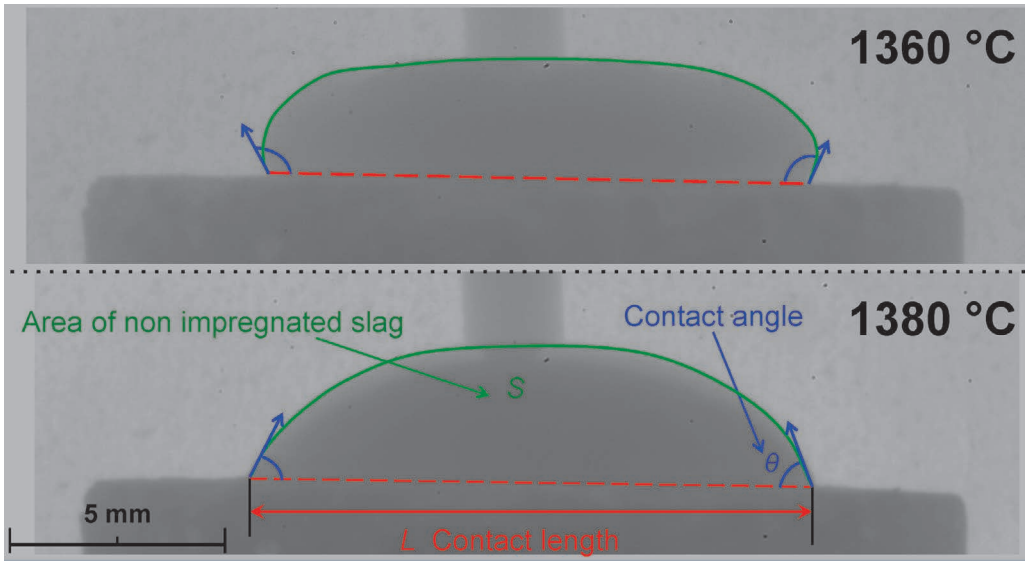

Fig. 10: Photo showing molten oxide pellet at 1360 °C and 1380 °C. Image processing allows determination of the contact length L between the molten oxide and the sample (red arrow), the molten slag area S (green area), and the contact angle θ (blue arrow).

Note that liquid phase, present at high temperature, made the bulk stiffness decrease and therefore facilitated the macroscopic deformation. Finally, the change in diameter of the top between the beginning and the end of the impregnation of the molten pellets, i.e. between 1380 °C and 1450 °C, was 63 % of the total change. The diameter expansion rate was 1 mm/h during this period. The change in diameter induced by the phase $CaO{\cdot}2(Al_2O_3,Fe_2O_3)$ can be assessed based on the difference of the change in diameter at the top (+2 %) with that at the bottom which is induced by the precipitation of $CaO{\cdot}6(Al_2O_3,Fe_2O_3)$ (-3 %). This gives about five points.

Finally, image processing was also performed on the pellets with Image J toolkit to assess the area occupied by the oxides on the image, the contact angle between the drop and the sample, and the contact length (Fig. 10). The three parameters are plotted from 1150 up to 1450 °C in Fig. 11. From 1150 to 1380 °C, the contact length decreased very slightly from the initial diameter of the pellets of around 13 mm. The area decreased in the same way indicating the pellets shrunk slightly owing to the melting that started at 1140 °C in agreement with the solidus temperature. The contact angle was constant at 90° until the pellets had melted sufficiently at about 1310 °C. From this temperature up to 1330 °C, the area started to decrease more quickly while the contact length started to increase. This indicates that the pellets transformed into a very viscous drop that did not wet the top surface of the sample since the contact angle increased sharply up to 140°. The contact angle decreased while remaining above 90° until the pellet melted quite completely right below 1380 °C. At the same time the drop started to spread on the top surface (contact length increase) and to densify (area decrease). At 1380 °C, the drop started to wet the sample and to impregnate the porous material. The contact length remained constant while both area and contact angle decreased. The slag area is the rest of slag that has not yet impregnated the porous material. Since the temperature rate is constant up to the dwell, the constant slope of the slag area indicates that the molten oxides impregnated the sample with a constant rate for 15 min and had completely impregnated it when the temperature reached the dwell (1450 °C).

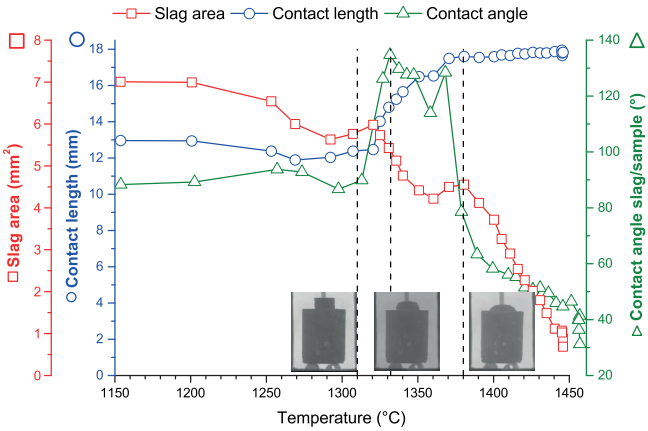

Fig. 11: Characterization of the impregnation kinetics.

IV. Conclusions

Contactless measurements have been developed to study the macroscopic deformation induced by phase transformations at high temperature. The device combines a high-temperature furnace fitted with a large window and a high-resolution camera. It allowed measurement of the deformation of a bauxite-based sample made of aggregates of millimetric size. The tests performed on sample alone allowed identification of the characteristic temperatures of phase transformations based on determination of the average diameter. The results were in good agreement with those obtained with other techniques. The thermal expansion coefficient of the material for temperature up to 800 °C; i.e. before the first phase transformation, which is the decarbonation, has been evaluated to $9.2 \times 10^{-6}\ K^{-1}$. At 1150 °C, when the liquid phase started to form, the liquid-solid sintering led to a change in diameter of 6 %. The sintering process effects vanished at 1450 °C when the expansive phase $CaO{\cdot}6(Al_2O_3,Fe_2O_3)$ precipitated and made

the diameter increase by 0.5 %. Adding pellets of oxides with a composition close to the molten phase enhanced the precipitation of $CaO{\cdot}2(Al_2O_3,Fe_2O_3)$, which led to the diameter increase of 5 %. The profile of the sample was related to the phase composition determined with SEM-EDX analyses. Image processing also allowed monitoring of the wettability of the molten oxides with the material and to describe the reactive impregnation mechanism. This technique highlighted the evolution of the physico-chemical properties of the slag and the interactions between the slag and the sample (wettability, time of impregnation) as a function of the temperature and the time.

In future, the *in-situ* optical measurement device will be used to investigate the deformation of refractories corroded by a slag, flux or salts. The intensity and the kinetic of the change in volume of impregnated refractory will be measured at high temperature. This approach will complete the kinetic of chemical corrosion investigations of refractories under extreme conditions.

Acknowledgments

The authors thank the Conseil Régional du Centre for financial support.

References

1 Zhu, S., Ding, S., Xi, H.a., Wang, R.: Low-temperature fabrication of porous SiC ceramics by preceramic polymer reaction bonding, *Mater. Lett.,* **59**, 595 – 597, (2005).

2 Blond, E., Schmitt, N., Hild, F., Blumenfeld, P., Poirier, J.: Effect of slag impregnation on thermal degradations in refractories, *J. Am. Ceram. Soc.,* **90**, 154 – 162, (2007).

3 Chotard, T., Soro, J., Lemercier, H., Huger, M., Gault, C.: High temperature characterisation of cordierite-mullite refractory by ultrasonic means, *J. Eur. Ceram. Soc.,* **28**, 2129 – 2135, (2008).

4 Ghassemi, A., Pak, A.: Pore scale study of permeability and tortuosity for flow through particulate media using lattice boltzmann method, *Int. J. Numer. Anal. Method. Geomech.,* **35**, 886 – 901, (2011).

5 Poirier, J., Qafssaoui, F., Ildefonse, J.P., Bouchetou, M.L.: Analysis and interpretation of refractory microstructures in studies of corrosion mechanisms by liquid oxides, *J. Eur. Ceram. Soc.,* **28**, 1557 – 1568, (2008).

6 Sako, E.Y., Braulio, M.A.L., Zinngrebe, E., van der Laan, S.R., Pandolfelli, V.C.: Fundamentals and applications on in situ spinel formation mechanisms in Al_2O_3-MgO refractory castables, *Ceram. Int.,* **38**, 2243 – 2251, (2012).

7 Stjernberg, J., Antti, M.-L., Nordin, L.-O., Odén, M.: Degradation of refractory bricks used as thermal insulation in rotary kilns for Iron Ore pellet production, *Int. J. Appl. Ceram. Tec.,* **6**, 717 – 726, (2009).

8 Stjernberg, J., Olivas-Ogaz, M.A., Antti, M.L., Ion, J.C., Lindblom, B.: Laboratory scale study of the degradation of mullite/corundum refractories by reaction with alkali-doped deposit materials, *Ceram. Int.,* **39**, 791 – 800, (2013).

9 Huber, T., Degischer, H.P., Lefranc, G., Schmitt, T.: Thermal expansion studies on aluminium-matrix composites with different reinforcement architecture of SiC particles, *Compos. Sci. Technol.*, **66**, 2206 – 2217, (2006).

10 Nam, T.H., Requena, G., Degischer, P.: Thermal expansion behaviour of aluminum matrix composites with densely packed SiC particles, *Compos. Part A: Appl. S.*, **39**, 856 – 865, (2008).

11 James, J.D., Spittle, J.A., Brown, S.G.R., Evans, R.W.: A review of measurement techniques for the thermal expansion coefficient of metals and alloys at elevated temperatures, *Meas. Sci. Technol.*, **12** R1, (2001).

12 Montanini, R., Freni, F.: Non-contact measurement of linear thermal expansion coefficients of solid materials by infrared image correlation, *Meas. Sci. Technol.*, **25**, 015013, (2014).

13 Zhang, X.R., Fisher, T.S., Raman, A., Sands, T.D.: Linear coefficient of thermal expansion of porous anodic alumina thin films from atomic force microscopy, *Nanoscale and Microscale Thermophysical Engineering,* **13**, 243 – 252, (2009).

14 de Bilbao, E., Prigent, P., Mehdi-Souzani, C., Bouchetou, M.L., Schimtt, N., Poirier, J., Blond, E.: Measurement of the volume expansion of SiC refractories induced by molten salt corrosion, *J. Ceram. Sci. Tech.*, **4**, 207 – 212, (2013).

15 de Bilbao, E., Prigent, P., Mehdi-Souzani, C., Bouchetou, M.-L., Schmitt, N., Poirier, J., Blond, E.: Measurement of the volume expansion of SiC refractories induced by molten salt corrosion. In: Proceedings of UNITECR 2013. Victoria, Canada, 2013.

16 Merzouki, T., Blond, E., Schmitt, N., Bouchetou, M.-L., Cutard, T., Gasser, A.: Modelling of the swelling induced by oxidation in SiC-based refractory castables, *Mech. Mater.*, **68**, 253 – 266, (2014).

17 Michel, R., de Bilbao, E., Poirier, J.: Recycling bauxite waste for the mineral Industry: phase transformations and microstructure during sintering, *Waste and Biomass Valori.*, 1 – 11, (2016).

18 Bale, C.W., Bélisle, E., Chartrand, P., Decterov, S.A., Eriksson, G., Hack, K., Jung, I.H., Kang, Y.B., Melançon, J., Pelton, A.D., Robelin, C., Petersen, S.: FactSage thermochemical software and databases — recent developments, *Calphad*, **33**, 295 – 311, (2009).

19 de Bilbao, E., Poirier, J., Dombrowski, M.: Corrosion of high alumina refractories by Al_2O_3-CaO slag: Thermodynamic and kinetic approaches, *Metall. Res. Technol.*, **112** 607, (2015).